Broadening of single quantum dot exciton luminescence spectra due to interaction with randomly fluctuating environmental charges

H. Kamada and T. Kutsuwa

NTT Basic Research Laboratories, NTT Corporation, 3-1 Morinosato-Wakamiya, Atsugi-shi, Kanagawa 243-0198, Japan

(Received 12 May 2008; revised manuscript received 1 September 2008; published 27 October 2008)

We studied line broadening of single-dot exciton emissions in terms of fluctuating interaction between the quantum dot (QD) exciton and environmental charges. We examined two types of QD excitons: one accompanied by trapped charge whereby the exciton line redshifts under the trapped charge population and the other nearly free from trapped charges. To avoid population decay of exciton—which results from multiple-carrier capture into the QDs, thereby leading to line broadening—and to highlight the effect of the fluctuating charges, we selected QDs that reject the capture of carriers in the barrier material. Interferometric correlation measurements of the single-dot emissions uncover the importance of the trapped charges near the QDs: The fluctuation of the Coulomb field caused by the trapping or detrapping of charges in point defects changes the autocorrelation function into Gaussian decay. A model dealing with the dynamics of the charge occupation driven by the thermally activated carrier capture and photoinduced carrier emissions is constructed consistent with the experiment. Upon temperature rise, the rate of the phase decoherence prevails over that of the charge fluctuation, and the autocorrelation function thereby turns to exponential. In contrast, in the QD nearly free from the trapped nearby charges, the autocorrelation decay obeys a simple exponential function, which is consistent with the absence of the fluctuating charge perturbation. Under an intense excitation, another decoherence due to the exciton or biexciton transition opens. We finally discuss the autocorrelation function in terms of the zero-phonon line and the phonon sideband.

DOI: 10.1103/PhysRevB.78.155324 PACS number(s): 78.67.Hc, 71.35.−y, 63.22.−m, 03.65.Yz

I. INTRODUCTION

The semiconductor zero-dimensional (0D) structure has long been a subject of interest not only in physics but also in practical device applications. The activity oriented toward the applications of semiconductor quantum dots (QDs) is now approaching a new apex following a number of successes in coherently controlling single excitons in isolated QDs by electrical and optical means.[1–6] Such approaches exploit the most distinct features of quantum confinement, namely, discrete density of states and long-lived coherence.[3–5,7–9] These specific features are often characterized by the lifetime of relevant states and their corresponding linewidth in the spectrum domain, which are determined by single-dot spectroscopy. Such measurements, in both the time and frequency domains, can in principle provide complementary information concerning short-term and long-term dynamics of the 0D states. Up to now, however, these measurements have yet provided a fully complementary view on the dynamical aspect of the exciton decoherence, although it is expected that the discrete density of states may substantially relax the complexities in the phase relaxation mechanisms.

In this paper we concentrate on the optical responses of QD excitons. The quantum phase of the excitonic state relaxes, being accompanied either by population relaxation or purely by relaxation of phase coherence.[10] Population relaxation of the excitonic states is accompanied by a change in energy corresponding to the absorption or emission of phonons or photons. The quantum phase can also be deteriorated without any energy change simply by a loss of coherence memory, and such processes are often referred to as pure dephasing.[11] It has been shown that the population relaxation of the lowest radiative state of QD excitons is driven mainly by spontaneous photon emission, which is often referred to as radiative decay.[12] An example is found in the radiative relaxation of excitons localized in potential minima in quantum wells, corresponding to island-shaped regions that are less confined relative to the surrounding,[13] where the phase coherence lifetime has been reported to be approximately equal to the spontaneous photon emission lifetime.[4,12,14] Another example is revealed by the four-wave mixing (FWM) technique on self-assembled QDs, where the phase relaxation lifetime of the excitonic states is close to the radiative lifetime.[7,9] Interestingly, both examples have attributed the dominant phase relaxation to the population decay due to the spontaneous photon emissions, although the lifetimes were substantially different, namely, 30–40 ps in the former case[4,12,14] and ~700 ps in the latter case.[7,9] These conclusions infer a predominance of the spontaneous emission over a wide range of QD spatial extent.

The exciton is a coherent superposition of an electron-hole pair excitation in all unit cells that covers its spatial probability distribution. Thus in this simple picture the oscillator strength strongly depends on the spatial extent of the QDs.[15] As the QD extent increases the exciton gains more oscillator strength because a larger number of unit cells coherently cooperates, as long as the coherence are longly maintained. Since the bulk interband dipole moment and the properties of the electron-hole envelope function primarily determine the exciton properties, the increasing oscillator strength in larger dots is due to much stronger Coulomb correlations between the electron and the hole because of the growing role of the Coulomb interaction. Keeping this in mind, let us look back at the above two cases. The excitons localized in the monolayer islands may be categorized as a

large dot and the other as a small dot. The radiative decay as the dominant decoherence mechanism infers that other mechanisms, such as the pure dephasing and phonon absorption into the excited states, are all ineffective irrespective of the degree of QD confinement from the limit having excitonic state energy separation of the order of millielectron volts to the other limit with that of a few ten millielectron volts. A consistent argument is that the rate of the phase relaxation due to the pure dephasing or by phonon absorption does not exceed the rate of the photon emission: As the confinement gets weaker to shrink the interlevel energy separation, the increase in the oscillator strength with increasing number of unit cells may boost the radiative decay rate, which may always prevail over the rates of other dephasing processes. If this is the case, in small QDs, the rate of the pure dephasing by phonon via virtual states must be slower than the radiative decay rate, ~700 ps,[7] and in large QDs, the sum—the phonon-mediated pure dephasing rate plus the phonon absorption rate into real excited states, which may be substantially fast compared to that in small QDs—must be smaller than inverse of 30–40 ps.[4,12]

In contrast to those observations, the spectral linewidth of the 0D exciton obtained by single-dot spectroscopy ranges from 20 to 100 μeV in full width at half maximum (FWHM).[16–19] Only a few reports have given linewidths corresponding to decoherence times longer than 100 ps.[20] Spectral resolution may not spoil the experiment since in the experiments conducted with a fairly nice resolution, the resolution fell to a range of ~20 μeV, which corresponds to 40 ps of the dephasing time. Most frequently observed radiative decay lifetimes measured by time-resolved photoluminescence (PL) decay experiments are longer than 200 ps;[9,16,21–25] the corresponding linewidth is less than 2 μeV. Since most of the reported linewidth γ values >30 μeV, the radiative decay as the predominant dephasing mechanisms is not at all supported by linewidth measurement results.[9,16] Although we will expect a criticism that the resolution of the linewidth measurements are not sufficient, it may be necessary to assume other broadening mechanisms to explain the broad distribution of the experimentally reported linewidth. One may attribute this disagreement to the neglect of the pure dephasing contribution. An earlier theoretical work on the basis of exciton-acoustic phonon interaction have, however, given a typical dephasing rate of 15 μeV in half width at half maximum (HWHM),[11] corresponding to about 100 ps in dephasing time, for larger QDs of a few ten nanometer at about 4 K. Decay dynamics observed in time-integrated FWM signal of a QD exciton ensemble is typically characterized by a fast initial decay (~ps) followed by a slow decay.[7] The former corresponds to the phonon sideband and the latter contributes to the zero-phonon line (ZPL). In more recent theories, both contributions are dealt altogether.[26–28] The theories well explain overall temperature dependence of the initial fast dephasing. However, the broadening of the slowly decaying part (ZPL) in a temperature range 4–50 K via two-phonon processes is very weak:[26] The experimentally observed temperature dependence of the ZPL broadening has yet been well explained. It has become clearer that acoustic phonons lead to broadening only via two-phonon processes and the effect is very weak at low temperatures.[26,27] Therefore the above-mentioned discrepancy in the slowly decaying part, which we focus in this paper, cannot be accounted for. Such a value does not account for the above discrepancy. For example, for a dot with a linewidth of ~30 μeV and a radiative decay lifetime longer than 300 ps, we may find an unknown dephasing contribution of ~15 μeV. For a dot, with a linewidth of ~70 μeV and a much longer radiative decay time constant, the discrepancy may be nearly 50 μeV. Another possible cause of additional single-dot exciton broadening is spectral wandering,[29,30] which may be a consequence of random interaction between the exciton and environment.[31] Representative origins may be interactions with point charges,[32] ionization of QDs,[29] unknown dipoles, or nearby QD excitons.[33] Among these, the effect of the Coulomb field originating from the point charge would be most significant because of its long-distance nature. It seems that such an effect proceeds with a time constant much longer than the lifetime of the exciton system, as reported:[29,31] The spectral wandering and/or luminescence intermittency[29,34] has been reported to occur on a time scale of the order of 10 ms to a second. Because multiple discrete spectral lines due to the wandering are not always clearly observed experimentally, the time constant of the spectrum shift may be much shorter than the typical measurement duration for single-dot spectroscopy. In such a case, the spectrum is diffused. Therefore, the spectral diffusion time constant—τ_w, with $\tau_w \ll T_{\mathrm{meas.}}$—is estimated, where $T_{\mathrm{meas.}}$ is the measurement time (possibly from hundreds of millisecond to a hundred seconds). It is now worth noting that the FWM measurement essentially relies on the dipole interference that is driven by two or more optical pulses sequentially delayed by arbitrary time that is shorter than the dipole decoherence lifetime. The results obtained by the FWM technique or any other techniques relying on the dipole interference are thus free from the long-term fluctuation whatever the origin of the fluctuation is. This leads to another inequality, $\tau_R \ll \tau_w$, where τ_R is the exciton radiative lifetime (from a few ten picoseconds to nanoseconds).

In this work, we studied broadening mechanisms of the single-dot emissions in terms of interaction between the QD exciton and environment. In order to study this, we strategically choose two types of QD excitons: one accompanied by trapped charge whereby the exciton line redshifts under the trapped charge population and the other nearly free from trapped charges. Also to avoid multiple-carrier capture into the QDs, we selected QDs that yield no luminescence under the excitation of carriers in the barrier material. This constraint favors stability of exciton population and enables highlighting the effect of the fluctuating charges near the QD. We performed interferometric correlation measurements[18,19,32,35] on the single-dot PL emissions on self-assembled QDs on (311)B face. By this method with an insertion of an interferometer in the single-photon detection, we observe linewidth variations from one QD to another, and we present evidence of environment effects. It is concluded that the Coulomb field produced by the carriers trapped in the point defects near the exciton under test, which is fluctuating by charge or discharge, give a substantial effect. This charge-exciton interaction gives rise to fast spectrum jumps, as well as to exciton emission line broadening. The single-

dot luminescence interferometry measurement reveals that the broadening is well described by the normal distribution, suggesting that the QD exciton is stochastically perturbed by many trapped charges, most probably in the barrier materials. In contrast, in the QD nearly free from the trapped nearby charges, the autocorrelation decay obeys a simple exponential function, which is consistent with the absence of the fluctuating charge perturbation. We observed that depending on the identity of dots and the excitation condition, the correlation decay exhibits a specific decay function, which is well described by the initial fast and subsequent slow decay. This behavior is explained by the zero-phonon line (slow part) and phonon sideband.

II. SAMPLES AND EXPERIMENTAL SETUP

A. Samples and techniques

QDs used in this study were disk-shaped InGaAs QDs formed via unique strain-driven spontaneous reorganization of a 3.5-nm-thick $In_{0.4}Ga_{0.6}As/Al_{0.5}Ga_{0.5}As$ heterostructure on (311)B face.[36] Details of the growth and the sample preparation are described elsewhere.[37] Noteworthy is that the QDs have no wetting layer because the Al-rich alloy, which was grown prior to the InGaAs film, spontaneously covers the In-rich nanoislands. Because of such spontaneous dynamics during the growth, none of the wetting layer can survive, and we do not need to overgrow the barrier material. Single-dot luminescence spectroscopy was performed by standard micro-PL measurements in the far field using a microscope objective lens (numerical aperture 0.5) in a confocal geometry as shown in Fig. 1(a). Two types of the excitation sources were used: a tunable continuous-wave Ti:sapphire laser and a diode-driven continuous-wave 532-nm laser. The former was used to resonantly excite discrete states of the QD excitons, and the latter to create electrons and holes in the barrier AlGaAs. The excitation beams were focused on the sample. For the Ti:sapphire laser, the spot size was about 2 μm in diameter. For the 532-nm laser, it was about 3 μm in diameter. The QD sample was mounted on the cold finger of a helium-flow cryostat for measurements down to below 4 K. The cryostat was accurately positioned using high-precision X-Y stages with a precision as fine as 0.05 μm. In order to isolate single QDs, the sample surface was processed with a thin dielectric film for protection and with a titanium film with submicrometer openings of various sizes, defined by electron-beam lithography and lift-off process. Favored by the thin dielectric (SiN) film, unwanted effect due to direct metal/semiconductor interfacing was effectively avoided. The excitation and the PL collection were made through the microscope objective lens. The PL was then dispersed by a triple monochromator with 640-cm focal length and detected either in a cooled Si-photon counting setup or with a cooled Si-charge coupled device array equipped with a monochromator. With this setup, we obtain a resolution variable from 30–40 to 150 μeV.

B. Quantum dots

The aim of the experiment here is to clarify how the fluctuating environment charges affect the QD spectrum. Hence

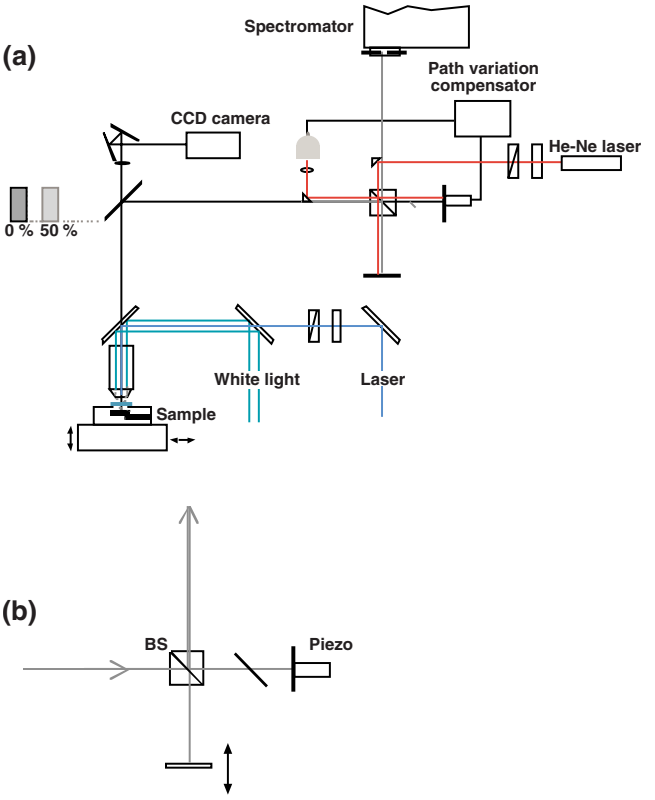

FIG. 1. (Color online) (a) Setup for the single-dot PL interferometry measurements: the single-dot PL passing through a Michelson interferometer followed by the spectrometer acting as a filter was detected by a single-photon detector. The first-order correlation function was obtained by measuring the PL count as a function of the delay. The interferometer was phase locked by moving a piezoactuator attached to the mirrors so as to maintain the interference of another He-Ne laser by feedback control electronics. (b) A thin glass plate was set in one of the interferometer arms, and only the PL beam was passed through it. Rotating the glass plate by a small angle gave a fine tuning of the relative phase between the two optical passes. Phase accuracy as good as $\lambda/20$ was achieved.

appropriate QDs must be carefully chosen. As mentioned, the Coulomb fields of the trapped charges may give the most significant effect. We have thus chosen two QDs: one exhibits no spectrum change under the excitation creating carriers in the barrier material (QD-1) and the other exhibits a substantial energy shift (redshift) under the similar excitation condition (QD-2). The spectrum shift is a signature of the presence of the proximity charged center: The charged center gives rise to a Coulomb field by which the exciton undergoes Stark shift. Throughout the experiments reported here, we adopted the above-barrier excitation as we wanted to intensively create carriers around the QD under test. On the other hand, the role of the resonant excitation is to create an exciton population in QDs. The excitonic emission of QD-1 is nearly isolated with no emission from the neighbor dots. On the other hand, the exciton emission of QD-2 is accompanied by two or three QDs near neighbor yielding luminescence emissions within an energy range of ~6 meV. These two QDs exhibit exciton emissions under the excitation resonant to excited states but do not exhibit emissions when the

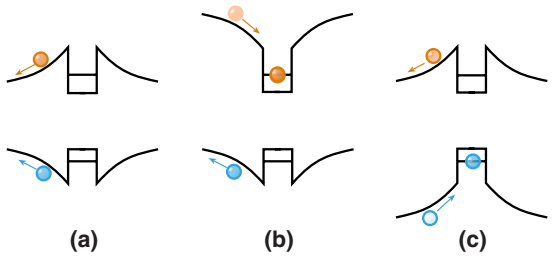

FIG. 2. (Color online) Variation in potential profile near quantum dot: (a) Potential profile repulsive for both electrons and holes, (b) repulsive for holes but attractive for electrons, and (c) that repels electrons and attracts holes. In (a), above-barrier excitation may not result in capture of either electron or holes. No exciton emission is expected. In (c) and (d), above-barrier excitation may cause trapping of either electrons or holes.

above-barrier excitation is adopted. This is likely due to surrounding potential profiles that prohibit capture of an electron and hole as a pair: Probable potential profiles are shown in Fig. 2. The first potential profile repels both electrons and holes in the barrier [Fig. 2(a)]: Thus, the above-barrier excitation results in the capture of neither electrons nor holes. The second potential is repulsive for holes but attractive for electrons [Fig. 2(b)], while the third one repels electrons and attracts holes [Fig. 2(c)]. In Figs. 2(c) and 2(d), the above-barrier excitation may cause trapping of either electrons or holes. Usual type of profile, which is not shown here, allows capture of electrons and holes. In contrast, in the above three potential profiles no exciton emission is expected under the above-barrier excitation. The excitation resonant to the intradot excited levels can, however, create excitons in the all three profiles.

The potential profile of our particular interest is the type (a). To study the environment effect, we first need to guarantee stability of the exciton population under test. Second, we need to create a distribution of electrons or holes in the neighborhood of the relevant QDs. In order to satisfy the first constraint, however, we need to avoid further capture of carriers into the QD, which would destroy the exciton population in the QDs under test. For guaranteeing these requirements are met, the specific nature of the potential profile (a) is most preferable. Therefore, we looked for candidates and selected two QDs, whose excitonic luminescence emissions are absent under above-barrier excitation and observed only under the resonant excitation. For examining the exciton emission under the presence of the above-barrier carriers, a weak above-barrier excitation simultaneously applied with the resonant excitation was adopted. The reason why variations arise from the potential profiles around QDs may be subtle material-composition fluctuations and resulting strain gradients around QDs. It is likely that such fluctuations and gradients result from the dynamical redistribution of indium atoms during the self-organization, which yields disklike quantum confinement structures. Detail of such phenomena may be substantially complex and still an open question.

The PL emissions of QD-1 and QD-2 are shown in Figs. 3(a) and 3(b), respectively. The exciton emission of QD-1 is 1.673 65 eV at 3.8 K under the resonant excitation at 1.7682 eV. The small peak at 1.668 46 eV is biexciton emission.

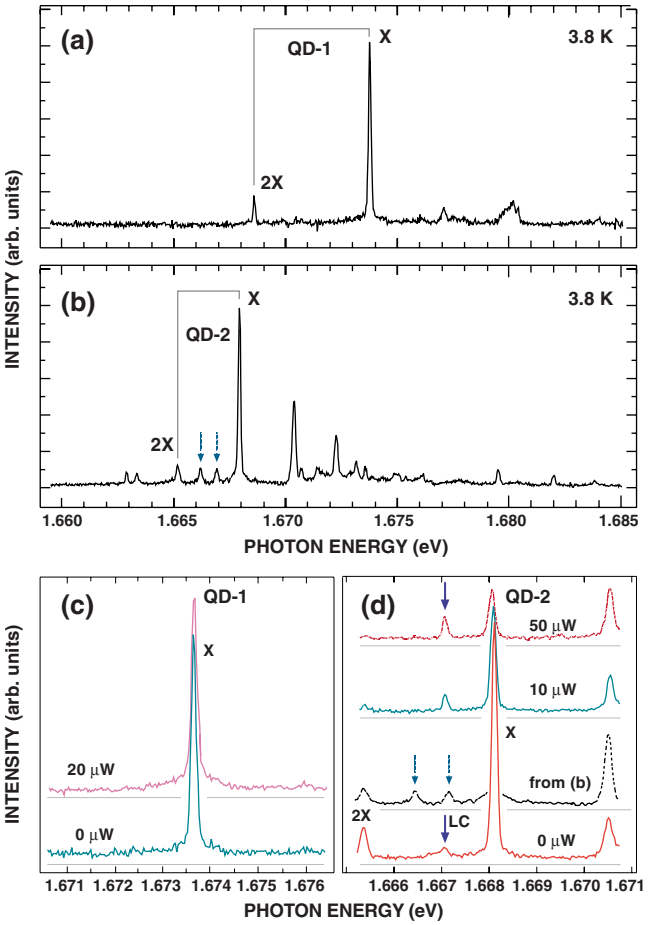

FIG. 3. (Color online) (a) PL spectrum of QD-1 under only resonant excitation (at 1.7682 eV). (b) PL spectrum of QD-2 exciton (X) under resonant excitation (at 1.6932 eV). The emission labeled 2X is the biexciton emission. (c) PL spectrum of QD-1 under the same resonant excitation as in (a) with weak above-barrier excitation (at 2.3308 eV); solid line is for the above-barrier excitation power 0 μW and broken line for 20 μW. (d) Spectrum variation in QD-2 under the same resonant excitation as in (b) without (solid line), with 10 μW, and with 50 μW of above-barrier excitation. Exciton emission intensity of QD-2 decreases with increasing above-barrier excitation intensity due to the shift in the excited-state resonance. The peak LC emerges when the barrier is simultaneously excited.

The former showed a linear dependency and the latter a quadratic dependency on excitation intensity. These two lines are well isolated from other emissions. In contrast, in Fig. 3(b), there are ten or more sharp lines besides the exciton emission of QD-2 at 1.6679 eV and the biexciton emission at 1.6652 eV (the resonant excitation energy of 1.6932 eV). The sharp lines are likely due to excitonic emissions from other QDs near QD-2. We confirmed that QD-1 and QD-2 show no PL emission when the excitation is above the barrier ($Al_{0.5}Ga_{0.5}As$). The above-barrier excitation simultaneously applied with to the resonant excitation was found to induce no substantial difference for QD-1 as mentioned [Fig. 3(c)]. In distinct contrast, it induced a redshift and substantial intensity decrease in the exciton emission of QD-2. We show in Fig. 3(d) the QD-2 emissions under the resonant excitation

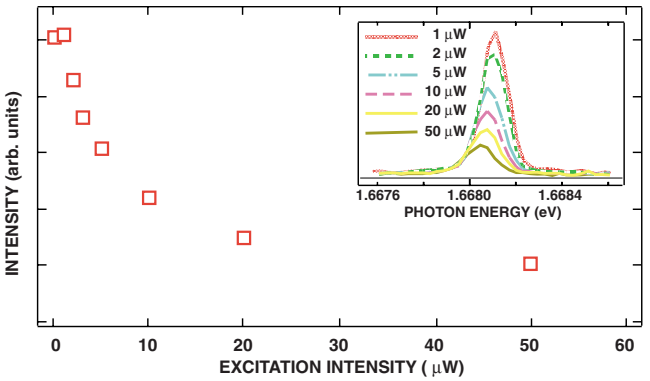

FIG. 4. (Color online) (a) Luminescence intensities of QD-2 under resonant excitation (at 1.6932 eV) with weak above-barrier excitation (at 2.3308 eV). Corresponding luminescence spectra for different above-barrier excitation powers (inset).

at 1.672 eV without and with the above-barrier excitation. Now the resonant excitation is redshifted by about 20 meV relative to that adopted in Fig. 3(b). Because of this difference, the peaks indicated by broken-line arrows disappear [in Figs. 3(b) and 3(d)], and a new line emerges [in Fig. 3(d)], while the exciton and the biexciton lines persist when excited only at 1.672 eV. The new emission line grows as the above-barrier excitation increases. As the excitation at 2.3308 eV is applied simultaneously with the resonant excitation, the exciton and the biexciton lines lose their intensities. In Fig. 4, we show the QD-2 exciton emission intensity as a function of the above-barrier excitation intensity. We attribute these to the excitonic level shift due to the electric field (Stark effect)[38–43] induced by free carriers or point charges in the neighboring QDs. The excited level, which we used for resonant excitation, may also shift under the local electric field. In fact, we noticed that the emission intensity recovered to that without above-barrier excitation when the laser frequency was slightly redshifted. We found that the frequency shift was about 30 μeV, while the redshift of the emission was 60.6 μeV. The fact that neither appreciable redshift in the PL emission nor the emission intensity decrease was observed in QD-1 with increasing above-barrier excitation intensity demonstrates a distinct contrast. The reason for such absence is attributed to absence of the nearby charged centers. It is then suggested that the redshift in QD-2 is due to electric field induced by such nearby charges, likely trapped in the lattice defects or impurities. Notice also that the PL emission peaks other than the QD-2 contribution at center do not lose their intensities under increasing above-barrier excitation and do not redshift. Therefore, they may trap electrons, holes, or both under the above-barrier excitation.

C. Single-dot PL interferometry

Single-dot PL interferometry measurements were performed by passing the PL through a Michelson interferometer before the spectrometer [Fig. 1(a)] to apply a first-order correlation measurement on single-dot exciton emissions. The PL beam was aligned parallel so as to keep its beam waist constant for a long-distance propagation to ensure interference visibility as good as 90%. To avoid unwanted reflection at optical component surfaces, all surfaces were antireflection coated. The interferometer was phase locked by moving one of the mirrors attached to a piezoactuator by feedback control electronics so as to maintain an interference of another He-Ne laser, which passed the same interferometer. The He-Ne laser beam was shifted vertically in beam poison relative to the excitation beam. A thin glass plate was set in one of the interferometer arm, and only the PL beam was passed through it. Rotating the glass plate by a small angle gave a fine tuning of the relative phase between the two optical passes.[5] The relative phase was stabilized to about $\lambda/130$ ($\lambda=633$ nm), and the phase accuracy as small as $\lambda/20$ was achieved. By varying the time delay τ, while maintaining phase locking, we recorded interference fringes of the single-photon events. The interferometric autocorrelation measurements revealed that line shapes of many QD excitons are not Lorentzian, although at a glance emission spectra seem Lorentzian.

III. RESULTS AND DISCUSSIONS

A. Gaussian broadening and temperature effects

First, we studied how environment charges around the QDs affect the first-order correlation function of the single-dot emission. Figure 5(a) displays a short-period fringe evolution of a single-dot PL emission (see inset, excitation at 1.6775 eV and emission at 1.6679 eV). We have chosen the exciton emission of QD-2, which appears together with other excitonic emissions from nearby QDs. The excitation at 1.6932 eV was resonant to a lower lying excited state to avoid multiparticle excitation, which is typically substantial as above-barrier excitation is adopted. The excitation energy was carefully chosen to minimize unwanted spectral contributions from the nearby dots. Nonetheless, three or four PL emissions attributable to nearby dots were visible probably because of coincidence of resonant absorptions. A visibility as good as 90% and a periodically oscillating intensity with a frequency, representing the center frequency of the recorded PL emission peak, were confirmed. The fringe evolution as a function of the delay t may be given by $I(\tau)=I_0[1+V(\tau)\cos(\omega\tau+\theta)]$, where (ω) is the center frequency, I_0 is the asymptotic intensity of the interference signal, $V(\tau)$ is the visibility contrast, and θ is the phase. Since the visibility contrast may decay with increasing τ, one can obtain the decoherence dynamics by measuring the functional $V(\tau)$. We plot in Fig. 5(b) the fringe contrast at 4 K as a function of t. It is clearly seen that it decays within 50 ps. One notices, however, that the overall dynamics does not obey a simple exponential function, which is frequently observed in the dynamics of single isolated systems. A test was then undertaken to know the decay function by trial-and-error fitting procedures. It was found that the decay of the fringe was most well fitted by Gaussian function, $C(\tau)=\exp(-\tau^2/\tau_c^2)$. Since we measured the dynamics of the single-dot optical responses, this seems very unusual: The Gaussian time evolution is typically observed for an ensemble, each of which is different in, for example, center frequency and decoherence dynamics. An example is a gas laser, whose broadening char-

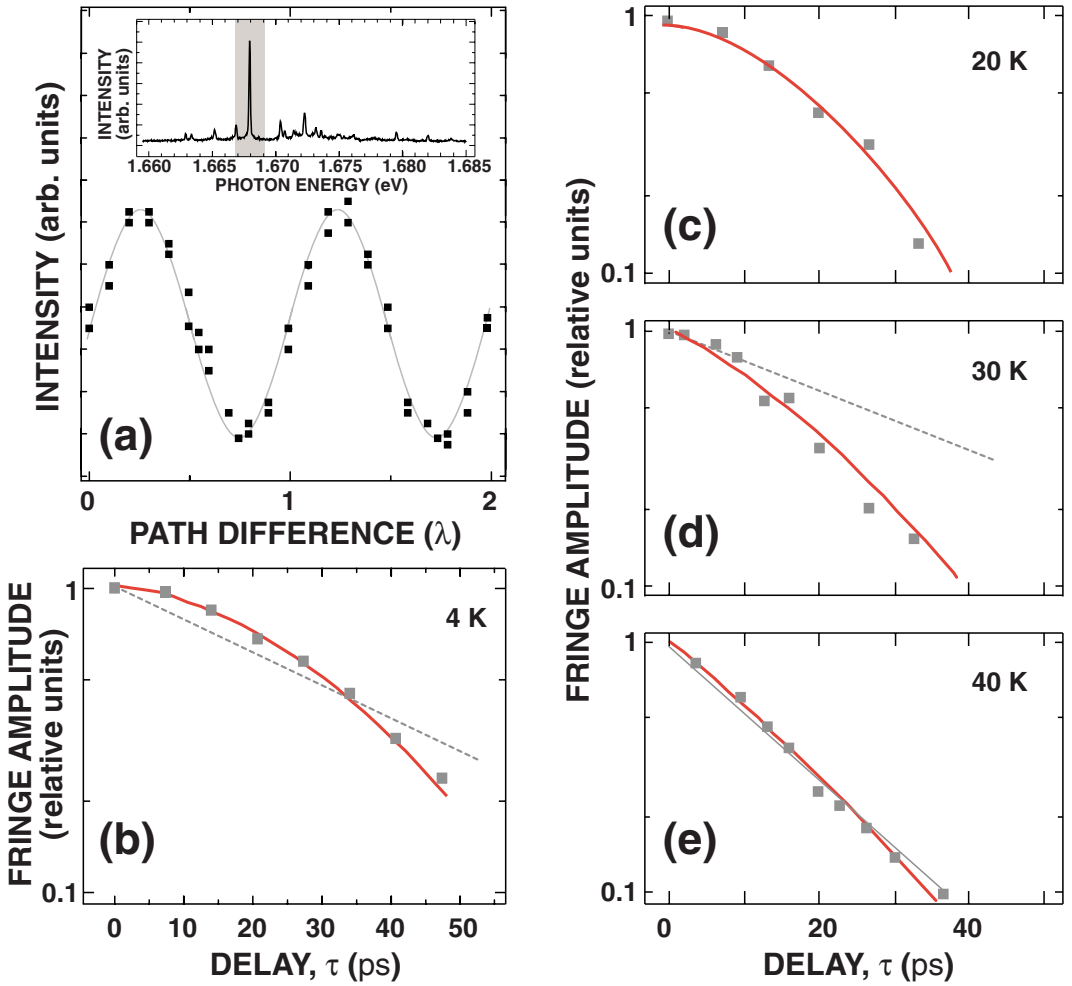

FIG. 5. (Color online) (a) Short-period fringe evolution of a single-dot exciton PL emission (1.6679 eV) under excitation at 1.6932 eV at 4 K. Relevant exciton emission is accompanied by emission lines from other nearby dots. The excitation was made resonantly to avoid multiparticle excitation. A visibility as good as 90% and a periodically oscillating intensity are confirmed. (b) Corresponding fringe amplitude variation for long-delay-time interval. Gaussian-type decay is visible. Fringe evolutions at (c) 20 K and at (d) 30 K. (e) At 40 K, exponential decay is observed. Interactions between the relevant exciton dipole and the environment at low temperature, which cause spectral diffusion, are suggested to result in Gaussian-type correlation function.

acteristics are determined by atomic collision.

To further elucidate whether or not this dynamical behavior is a universal tendency in the relevant QD, the temperature dependence of the interferometry response was studied for the same QD. Shown in Figs. 5(c)–5(e) are the fringe amplitude decays measured at 20, 30, and 40 K, respectively. Notice that the fringe decay function seems Gaussian for temperatures lower than 40 K. At 40 K, the amplitude decays faster and the decay function is well fitted by the simple exponential function $C(\tau)=\exp(-|\tau|/\tau_c)$ instead of a Gaussian that fits well the evolution at lower temperature. In Fig. 6, we summarize the corresponding linewidth (half width) as a function of temperature. It is worth pointing out that below 40 K, the time constant increases with a slope of $\sim 0.45\ \mu\mathrm{eV/K}$. A time-resolved measurement on the relevant QD exciton emission revealed a radiative decay lifetime of 260 ps (corresponding half width $\gamma_R/2\sim 1.3\ \mu\mathrm{eV}$). Thus, the radiative contribution to the linewidth is negligible.

The temperature dependence of linewidth is often understood in terms of acoustic-phonon-mediated dephasing at low temperature (<50 K), and abrupt broadening above 50 K represents population decay due to scattering by longitudinal optical phonons. The increase in linewidth below 40 K in Figs. 5 and 6 may then be due to acoustic-phonon scattering. Since the simple exponential decay function, which correspondingly gives Lorentzian line shape in the frequency spectrum, is recovered above 40 K, it is strongly suggested that the random interactions between the relevant exciton dipole and the environment charges at low temperature cause the broadening. In this view, the unknown interaction may cause the broadening on a time scale substantially different from that of the dipole-phonon interaction. The Gaussian distribution further suggests that such interactions stochastically perturb the exciton dipole, and because of this, the exciton emission is broadened according to the Gaussian distribution even though one is observing a single dot. It has been theoretically predicted that virtual transitions due to LO phonons may give rise to a Gaussian line shape.[44] However, the Gaussian broadening by such a mechanism is ineffective in our temperature range $T<50$ K and becomes effective at

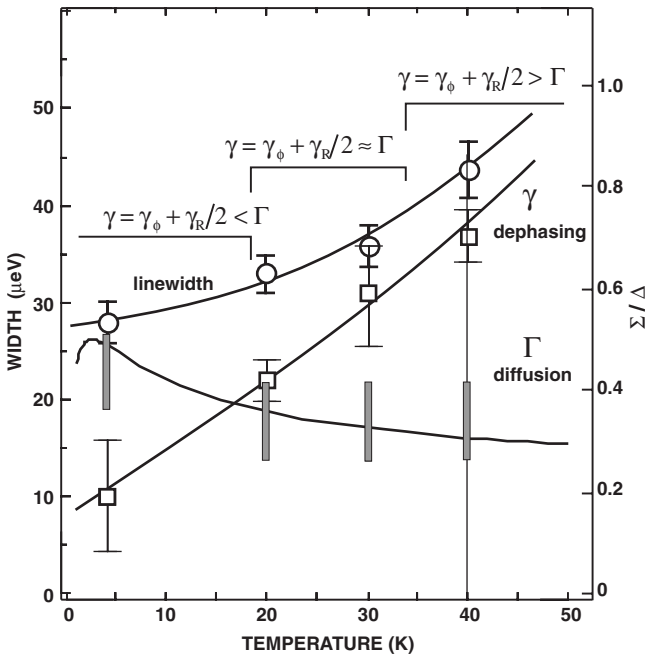

FIG. 6. Inverse of characteristic time constant, $1/\tau_c$, as a function of temperature (open circles). Dephasing contribution γ (for left axis) and spectrum diffusion contribution Γ (for left axis and for right as Σ/Δ) determined through the fitting to the decays are also shown as open squares and elongated shaded rectangles, respectively. Below 40 K, the time constant increases with a slope of 0.45 μeV/K. The simple exponential decay function is recovered above 40 K, suggesting that below 40 K spectral diffusion prevails over dephasing, and dephasing dominates above 40 K.

elevated temperature, say $T>100$ K. In fact, Uskov *et al.*[44] predicted a linewidth contribution as low as 10^{-6} meV at 10 K. By contrast, the Gaussian broadening contributes substantially. Thus, we may safely attribute the result here to the stochastic perturbation. Hereafter, we refer to the broadening due to the dephasing as the dephasing contributions. A broadening contribution due to the other random interactions was estimated from the temperature where the correlation function changes from Gaussian to exponential. This crossover temperature is about 20–30 K. In this temperature range, the dephasing contribution and the random fluctuation may give nearly equal contributions. One thus estimates the corresponding width due to the random processes as 15–25 μeV at around the crossover temperature.

The existence of a fluctuating environment around the QD originates from the presence of charges in impurities or in defects in the surrounding material. A single perturbing center induces a Stark shift of the QD exciton emission: In this simple case, since the presence or absence of the charge gives two energies of the exciton, the situation is described by binomial distribution statistics. As we introduced probability q, where one finds the center is charged and thus the spectrum is shifted by Δ, the distribution function is given by $w_n(m)=\binom{n}{m}p^{n-m}q^m$, where one finds the shifted spectrum m times in n trials. The mean value of m is $\langle m\rangle=nq$ and the dispersion is $\sigma^2=nqp$. Now for convenience we introduce the quantity $x=(m-\langle m\rangle)/n^{1/2}$ and transform $w_n(m)$ into $w(x)$. It is well known that $w_n(m)(n\to\infty)=(2\pi\langle m\rangle p)^{1/2}e^{-(m-\langle m\rangle)^2/2\sigma^2}$, where $\sigma^2=\langle m\rangle p$. The distribution can be easily rewritten in terms of energy by assuming ergodicity. We may regard q as the occupancy of the charge in the trap, f. Thus the dispersion may be written as $\Delta[(1-f)f]^{1/2}$. For detecting the charge trapping or detrapping from the exciton energy shift, each charge state must stay at least for an interval $\delta t\approx\hbar/\Delta$ (for example, 22 ps for 30 μeV). Because we use the exciton spontaneous emission, our resolution is limited by its lifetime and the corresponding width (3.3 μeV for 200 ps and 0.66 μeV for 1 ns). The trial interval and the trapping or detrapping correlation time must to be longer than the lifetime. We extend the model to the case where the fluctuating reservoir consists of two uncorrelated perturbing centers, which individually induce a Stark shift Δ_i of the quantum dot line and whose distribution functions are described by the mean values and the dispersions, $\{\langle m_1\rangle,\Sigma_1\}$ and $\{\langle m_2\rangle,\Sigma_2\}$. Now we have four possible configurations of the occupied or empty traps. The exciton emission energy varies as a discrete variable; each value corresponds to a particular configuration and has a probability. However, as the two traps are mutually uncorrelated, the distribution function of the two-trap system can again be described as Gaussian by the addition theorem of the normal distribution. The new distribution is then characterized by $\{\langle m_1\rangle+\langle m_2\rangle,\Sigma_1+\Sigma_2\}$. Extension to N-trap system can be similarly made, then the distribution is described by $\{\langle m_1\rangle+\langle m_2\rangle+\cdots+\langle m_N\rangle,\Sigma_1+\Sigma_2+\cdots+\Sigma_N\}$. The resulting distribution can be easily rewritten in terms of energy. The width parameter Γ is the sum of the dispersion of the N traps, each of which has the expression $\Delta_i[(1-f_i)f_i]^{1/2}$. The occupancy f_i depends on a characteristic capture and emission rates, which may change as temperature or excitation intensity is altered. The exciton spectrum is a convolved Lorentzian with regard to the Gaussian, which represents the distribution of the perturbed exciton center frequencies.

We may describe how random fluctuations in frequency would influence the optical transition line shape in a quantum mechanical framework. The line shape will be obtained from the dipole correlation function for the electronic transition. We will find the line shape function for a Gaussian-Stochastic model for random fluctuations in the transition frequency ω_0. The time dependence to the transition energy reflects random fluctuations about average value: $\omega(t)=\langle\omega_0\rangle+\delta\omega(t)$ and $\langle\omega_0(t)\rangle=0$. The fluctuations in ω allow the system to go through a Gaussian distribution of transitions frequencies characterized by a variance: $\Delta=\langle\delta\omega^2\rangle^{1/2}$. The time scale of the fluctuations is characterized by a correlation time, $\tau_c=\int_0^\infty\langle\delta\omega(t)\delta\omega(0)\rangle/\Delta^2$. Following Anderson and Weiss,[45] the dipole moment may be assumed to coupled to the frequency fluctuation $\omega(t)$ via

$$\frac{\partial\mu}{\partial t}=-i\omega(t)\mu, \tag{1}$$

$$\mu(t)=\mu_0\exp\left[-i\int_0^t d\tau\omega(\tau)\right].$$

The formal solution to the equation is

$$\mu(t) = \mu_0 \exp\left[- i\langle\omega\rangle t - i\int_0^t d\tau \delta\omega(\tau) \right]. \quad (2)$$

We introduce a time-dependent expectation value $F(t) = \langle \exp[-i\int_0^t d\tau \delta\omega(\tau)] \rangle$, then

$$\langle \mu(t)\mu(0) \rangle = \mu^2 e^{-i\langle\omega\rangle t} F(t). \quad (3)$$

We expand $F(t)$ as cumulant expansion of average to obtain

$$F(t) = \exp\left[- i\int_0^t d\tau (t-\tau) \langle \delta\omega(\tau)\delta\omega(0) \rangle \right], \quad (4)$$

which is a term that survives for a system with Gaussian statistics to the fluctuations. Therefore, the frequency fluctuations are described by a correlation function $\langle \delta\omega(\tau)\delta\omega(0) \rangle$, where the correlation time is $\tau_c = \int_0^\infty dt \langle \delta\omega(t)\delta\omega(0) \rangle / \Delta^2$. We calculate the line shape assuming that the correlation function decays exponentially such that $\langle \delta\omega(t)\delta\omega(0) \rangle = \Delta^2 \exp[-|t|/\tau_c]$. Then

$$F(t) = \exp\{ - (\Delta\tau_c)^2 [\exp(-|t|/\tau_c) + |t|/\tau_c - 1] \}. \quad (5)$$

In a long correlation time limit, where $t \ll \tau_c$, the exponential function above can be expanded only to second order, thus $\exp[-|t|/\tau_c] \approx 1 - |t|/\tau_c + t^2/2\tau_c^2$. The line shape function is thus proportional to $\int_0^\infty dt e^{-i\omega t} e^{-i\langle\omega\rangle t} F(t)$ and is rewritten as

$$\int_{-\infty}^{\infty} dt e^{i(\omega - \langle\omega\rangle)t} e^{-t^2\Delta^2/2} = e^{-(\omega - \langle\omega\rangle)^2/(2\Delta)^2},$$

which is Gaussian. When the correlation time is short so that $t \gg \tau$, $\exp[-|t|/\tau_c] + |t|/\tau_c - 1 \approx |t|/\tau_c$. Now, the line shape is Lorentzian being proportional to

$$1/[- (\omega - \langle\omega\rangle)^2 - (\Delta^2\tau_c)^2]$$

since $F(t) = \exp[-\Delta^2\tau_c t]$. The above two extreme cases serve as a phenomenon known as "motional narrowing:" Even with a broad distribution of frequency, if the system undergoes all of these frequencies on a time scale short compared to the inverse of the distribution ($\Delta\tau_c > 1$), then the resonance line will be "motional narrowed" into a Lorentzian line. A fully quantum mechanical formulation for a formula such as Eq. (5) is given from the quantum Heisenberg equation for the dipole operator, which is given in Ref. 41. In the experiment, the autocorrelation of the field $E(t)$ for the delay τ is given as $S(\tau) = 1 + \mathrm{Re}[G(\tau)e^{-i\omega\tau}]$, where $G(t) = \langle E(t)E^*(t-\tau) \rangle / \langle E(t)E^*(t) \rangle$ and $\langle\ \rangle$ represents integration from −infinity to +infinity. The Fourier transformation of $G(t)$ gives the power spectrum $s(w) = |E(\omega)|^2$. We calculate the convoluted spectrum $s(w)$, then Fourier transform it to obtain $G(t)$. Therefore, we have the amplitude of the interference term as $e^{-\gamma\tau} e^{-\Gamma^2\tau^2/2}$, where γ and Γ are, respectively, the dephasing rate and the distribution width. We tried fitting the amplitude decay functions with the above formula. In Fig. 5, the results of the fitting are shown as solid lines. The Gaussian to exponential transition from 4 to 40 K is well reproduced. By the fitting, we also have γ and Γ for each decay function. They are plotted in Fig. 6. Note that γ and Γ intersect around 20 K, concomitant with the crossover temperature predicted before. The contribution due to the dephasing, γ, increases linearly with temperature, and the slope is about 0.73 μeV/K. On the other hand, the spectral diffusion contribution Γ does not show appreciable temperature dependence or it weakly decreases as temperature rises. Although we do not know the exact mechanism of the charge traping or detrapping, we may consider a situation described as follows. We consider electrons as majority carriers, and perturbing charges are trapped electrons. We estimated an electron concentration of 10^{13}–10^{14} cm^{-3} at 4 K. One may wonder trion formation under a residual concentration of electron. We observed, however, a small splitting less than 20 μeV, very likely due to long-range electron-hole exchange interaction through small anisotropy in shape. If they are trions, we do not expect any splitting because two electrons are paired off. Thus, we can safely disregard trion formation. For simplicity, we consider electrons as majority carriers, and perturbing charges are trapped electrons. In the steady state, the electron occupation of the trap is determined by the rates of the competing capture and emission. The former is written as $n\langle v_e \rangle \sigma_e$, where n, $\langle v_e \rangle$, and σ_e are, respectively, the concentration, the thermal velocity, and the capture cross section of the electron.[46] Therefore, the capture rate is written as $c_e = \sigma_e (3k_B/m_e^* m)^{1/2} n T^{1/2}$, where m, m_e^*, and T are the electron mass, the electron effective mass, and the absolute temperature, respectively. The emission rate depends on the depth of the trap from the band edge and is thermally activated: it is given from the principle of detailed balance as $e_e = [\sigma_e \langle v_e \rangle N_D / g] \exp(-\Delta E / k_B T)$, where N_D and g are the density of states in the band to which the carrier is emitted and the degeneracy.[46] Typically, the pre-exponential factor $\nu_\infty = \sigma_e N_D / g$ is in the range of 10^8–10^{14} sec^{-1}. Therefore, in equilibrium in a temperature range of 40–50 K, $c_e \gg e_e$, and thus the occupancy of the trap is constant until the trap is very shallow from the band edge. Upon minority carrier excitation, however, the capture of the minority carriers competes with that of the majority carriers. Otherwise, the photoexcitation induces carrier emission well known as photoinduced current or photocapacitance change in the point defect spectroscopy. We take into account electron capture as $nv_e\sigma_e$ and hole capture as $pv_h\sigma_h$. Also, we consider photoinduced electron emission, which may be written as $n_o = \sigma_o \phi$, where σ_o and ϕ are the optical cross section and the photon flux, respectively. Rate equation describes such a situation and is written as $df/dt = (c_e + n_o)(1-f) - c_h f$. Under constant density optical excitation, the steady-state electron occupancy f of the trap is $(c_e + n_o)/(c_e + c_h + n_o)$. When the resonant excitation to the QD discrete level is applied, we disregard c_h because the excitation energy is below the barrier band gap. On the other hand, we need to include c_h under the above-barrier excitation. For the experiment in Fig. 5, we thus use $f = c_e/(c_e + n_o)$. Now we regard this as representative occupancy averaged over all the traps. Similarly, we consider representative Stark shift Δ. We can estimate the photoinduced emission rate from the photon flux, and it is about 10^5 sec^{-1}. As mentioned, the dispersion is written as $\Sigma = \Delta[(1-f)f]^{1/2}$. Therefore, we expect that Γ in Fig. 6 has the same temperature dependence as Σ/Δ. By varying the cross sections and Δ we fitted the experimental variation in Σ/Δ, where a constraint $s_e < 10^{-15}$ cm^2 was introduced to rationalize the carrier capture model.[46] The result of the fitting is

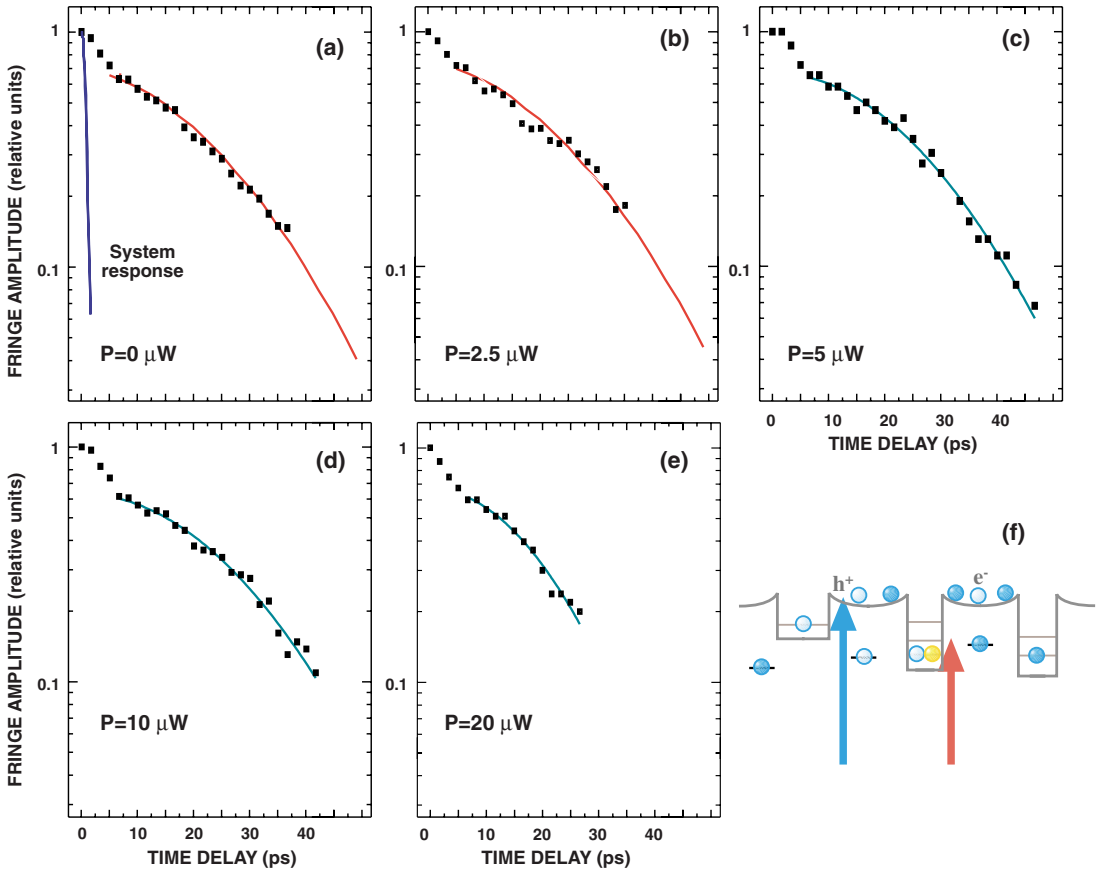

FIG. 7. (Color online) Luminescence autocorrelations of the QD-2 exciton under resonant excitation (100 μW at 1.6775 eV) with weak above-barrier excitation (at 2.3308 eV); change is shown for a variety of above-barrier excitation powers. The dynamics does not obey a simple exponential function. The functional does not seem to be Gaussian either: The dynamics exhibits faster decay of 30%–40% in the first 7–8 ps, then a weak shoulder, followed by Gaussian-type decay. Overall, the decays seem constant at about 18–20 ps. The decay remains similar for (a) 0, (b) 2.5, (c) 5, and (d) 10 μW, but for (e) 20 μW it becomes faster. The figure (f) schematically represents the resonant excitation to the QD exciton under test and the effect of the above-barrier excitation leading to carrier generation in the barrier and trapping into the traps and neighboring QDs. Blue solid line in (a) is the system response function.

shown in Fig. 6 as Σ/Δ (for the right vertical axis), where we adopted the background barrier electron density of 10^{14} cm^{-3}, $\sigma_{eo}=1.3\times10^{-17}$ cm^2, $\sigma_e=6\times10^{-15}$ cm^2, and $\Delta=66$ μeV. The temperature dependence of Σ/Δ well explains Γ's dependence.

B. Effects of above-barrier excitation

1. Spectral diffusion

It is now worth recalling single-dot spectrum broadening under the barrier excitation,[47] where broadening with a factor of up to 2 was observed under an excitation density as low as 0.5 W/cm^2. It was concluded that such an efficient broadening could be due to multiparticle excitation in QDs, such as electrons, holes, and electron-hole pairs. However, in the present experiment, the multiparticle excitation is significantly suppressed because of the potential profiles. Thus, for example, it is expected that excitation of more than one exciton following the first exciton creation, which results in a biexciton, may not be allowed. The remaining cause of the exciton emission line would be due to fluctuating Coulomb fields from the point charges in the near neighbor environment. From this viewpoint, we conducted correlation decay measurements on QD-2, which exhibits the spectral shift in the presence of the carriers in the barrier material. The results may then be compared to a similar experiment on QD-1, which is considered to be free from trapped charges in its proximity.

Figure 7(a) displays five fringe decays at 3.8 K of the QD-2 exciton, each of which corresponds to different above-barrier excitation intensities (at 2.3308 eV), namely, 0, 2.5, 5, 10, and 20 μW. The resonant excitation energy is 1.6775 eV, different from that in Fig. 3. Again, this energy was chosen to minimize unwanted spectral contributions from other dots, which may appear under this resonant and the above-barrier excitations. The fringe contrast as a function of τ reveals again decays in 20–30 ps. The decay times observed here are not substantially different from those in Fig. 5. The resonant excitation energy here is different from before: The present excitation energy is lower by about 91 meV. Nevertheless, the decay does not change substantially. This is in contrast with the reported observation that the decay lifetime decreases for higher excess excitation energies[35] because of the increasing excited carrier densities. The absence of such behavior is attributed to the special

potential profiles around the QDs strategically chosen, which may be insensible against the carrier generation. One notices, as before, that the dynamics under the higher above-barrier excitation intensities do not obey a simple exponential function. The functional, however, does not seem to be Gaussian either: The dynamics exhibits faster decay of 30%–40% in the first 7–8 ps, then a weak shoulder, followed by a Gaussian-type decay. Overall, the decays seem constant at about 18–20 ps. Such unusual decays have been reported[19,32] and attributed to background broad luminescence contributions from bulk or two-dimensional materials. We can, however, exclude such attribution. First of all, the fairly large decay portion as large as 30%–40% contributes to this initial fast decay. Second, such attribution is excluded because a 1-meV shift of the center energy of the measurement window to an energy range, where no excitonic peak is observed, gave us a very weak signal and such initial decay was not observed. The observed initial decay is sufficiently slower than the measurement time resolution. The system response function is shown in Fig. 7(a). A similar decay dynamics has been observed in time-integrated FWM signal of a QD exciton ensemble, which is characterized by a fast initial decay (~ps) followed by a slow (>400 ps) decay.[7] It was suggested that the former corresponds to the phonon sideband, and the latter contributes to the central part of the exciton absorption spectrum, which is the zero-phonon line. The photoexcitation of the exciton can proceed with the creation or annihilation of phonons, and such processes contribute to the sidebands.[48] It is tempting to explain our observation in terms of a similar mechanism. At present, however, we cannot give any conclusive attributions about the origin of the initial decay. Let us then focus on the remaining decay portion that follows and bows for longer delay. After the first 10 ps, the decays seem Gaussian. The decay remains very similar for 2.5, 5, and 10 μW, but for 20 μW it becomes faster. This is ascribed to increasing frequency of charge fluctuation near the dot due to the increasing rate of the carrier creation. The Gaussian-type decay dynamics reflects the random fluctuation, which seems to increase for higher excitation. But its rate does not increase substantially. This is in contrast to the exciton line broadening of the QDs under the above-barrier excitation, which we formerly reported for QDs that allow multicarrier capturing.

The above results may be compared with the QD exciton without any energy shift under the above-barrier excitation simultaneous to the resonant excitation. For this comparison, we undertook a similar measurement of the exciton emission in QD-1. We present the results in Fig. 8, where the luminescence autocorrelations of the QD-1 exciton under resonant excitation (50 μW at 1.7682 eV) with weak above-barrier excitation and the decay for 0, 5, and 10 μW of the above-barrier excitation power are given. As depicted in the inset (bottom left), carriers in the barrier may not be trapped in QD-1 because of the potential profiles. Notice in Fig. 8 that regardless of the increasing above-barrier excitation powers, the autocorrelation functions are exponential and nearly identical, keeping the lifetime of 18 ps (the corresponding half width of 36 μeV). We believe that the constant decay time is due to the stable QD-1 exciton, which is less perturbed because of the absence of the charges within a distance of less than 10–20 nm. However, we still regard the broadening to be due to the randomly fluctuating environment charges because the observed exponential decay only infers that $\Gamma < \gamma$ (or $\Gamma \leq \gamma/2 \approx 12$ μeV), as we saw in the case of Figs. 5 and 6. Such situation can be met when the remote charges are located at a distance longer than 100 nm. As we compare the behaviors of QD-1 and QD-2, it is suggested that the perturbation due to the nearby trapped charge probably at a close distance (<10–20 nm) seems significant, giving rise to the clear Gaussian amplitude decay as in Fig. 7. Other than the trapped charges, trapped carrier in the nearest-neighbor QDs is another candidate. As carriers are trapped as excitons, they give rise to dipole-dipole coupling to the QD-2 exciton that we examined. The strength of such interaction is, however, expected to be too small because energy differences between the QD-2 emission and the others are larger than ~2 meV, as seen in Fig. 3, and the dipole-dipole coupling is known to be effective only when two dipoles are nearly resonant. Note that we observed another emission line other than that of QD-2, which is indicated by the solid-line arrow in Fig. 3(d); it grows as the

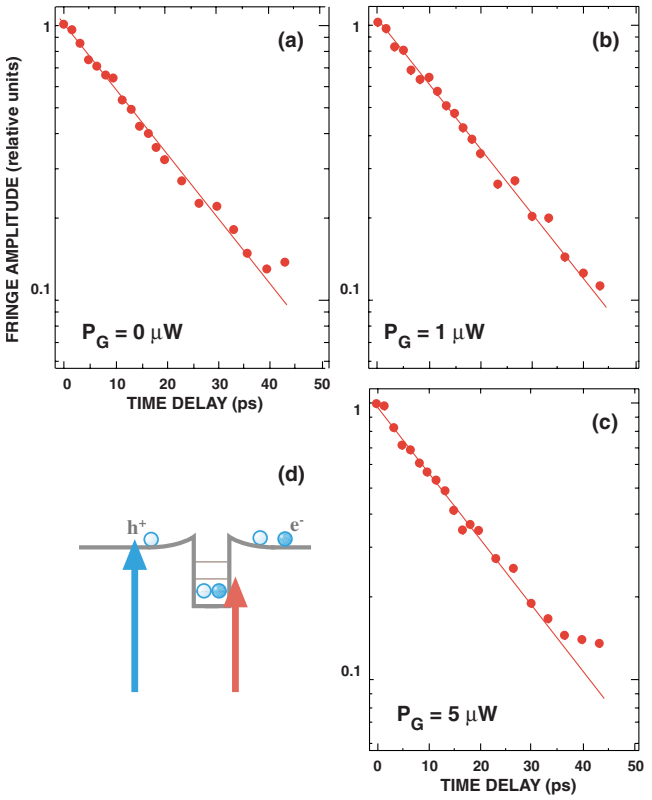

FIG. 8. (Color online) Luminescence autocorrelations of the QD-1 exciton under resonant excitation (50 μW at 1.7682 eV) with weak above-barrier excitation (at 2.3308 eV); Change is shown for the absence, 5 μW, and 10 μW of above-barrier excitation power. Regardless of the increasing above-barrier excitation powers, the autocorrelation function obeys the simple exponential decay function with a constant characteristic lifetime. The inset (bottom left) schematically represents the resonant excitation to the QD exciton under test and the effect of the above-barrier excitation leading to carrier generation in the barrier. Because of the potential profiles around the QD-1, no trapping of carrier into QD-1 occurs.

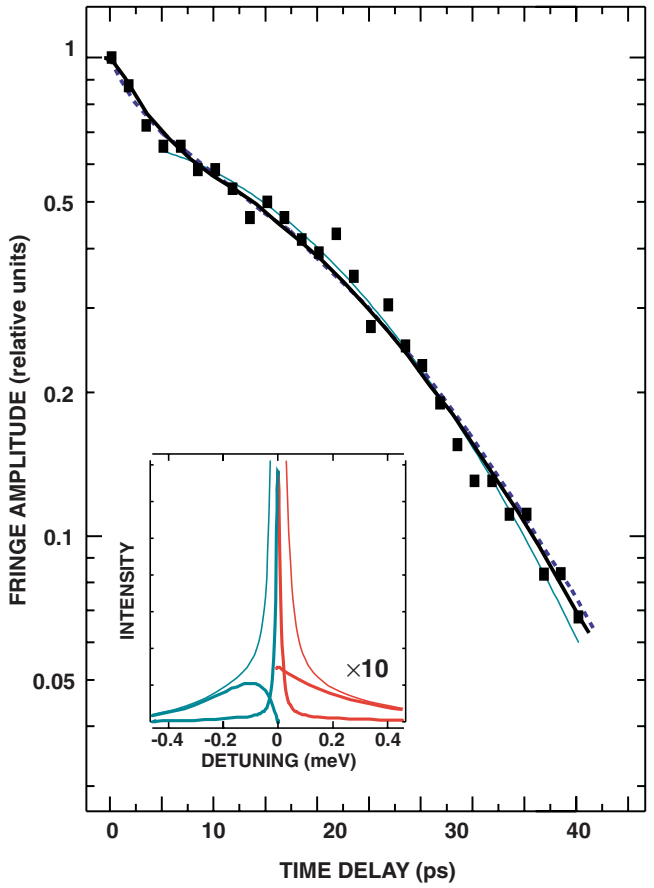

FIG. 9. (Color online) Magnified view of the fringe amplitude in Fig. 7(d). The decay function is characterized by steeper decay at the first 7 ps and a slow down of decay in the subsequent delay. A Gaussian broadened decay is shown by a thin solid line. Decay calculated for ZPL and sideband with model A (b) is shown as a broken line (thick solid line), and the corresponding spectrum (left with model A, right with model B) is shown in the inset.

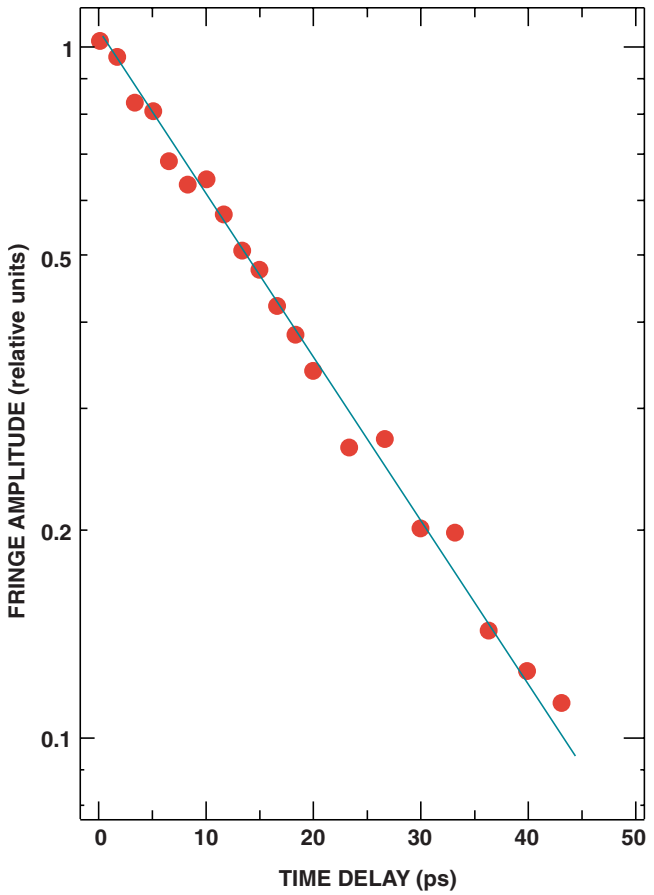

FIG. 10. (Color online) Magnified view of the fringe amplitude in Fig. 8(b). The decay function is well approximated by exponential decay. Fitted exponential decay is shown as solid line.

above-barrier excitation increases. This then suggests that this is due to an exciton trapped by a charge in the neighboring QD. It is estimated, however, that the electrons or holes trapped in the nearest-neighbor QD (about 120–150 nm in our sample) only cause an electric field of as much as only 50–100 V/cm. Therefore, we conclude that the primary candidate of the perturbing center is a charge trapped in a defect located very close to the QDs under test. The remote charges (100 nm), which are also trapped in defects, are secondary candidates.

C. Effects of fluctuating neighboring charges

The above results for QD-2 as compared to QD-1 suggest perturbations from the neighboring charges. A magnified view of the data in Fig. 7(c) is shown in Fig. 9. Similarly, the data in Fig. 8(b) is magnified in Fig. 10. Apparently, the very specific decay function in Fig. 9 is markedly different from that in Fig. 10. We now focus on the Gaussian decay part. Thus, as before, we tried a fitting in $\tau > 7$ ps with Voigt function, which is the convolution of Gaussian and Lorentzian functions. The results of the fitting are shown in Fig. 7. The fitting demonstrates that the characteristic decay functional in $\tau > 7$ ps is well reproduced. Parameter sets $\{\gamma, \Gamma\}$ obtained by the fitting are summarized in Fig. 11. Since we used QD-2 and we know that γ and Γ are competing, they are again similar to each other. Because of this, errors of the fitting are relatively large. Thus, the data are represented with error bars. The increase in Γ for the larger power can be understood as the increase in the frequency of the fluctuation, which can be reasonably accepted to be a result of more frequent capture of the barrier electrons and holes. However, the increase is only by a factor of 1.5. In contrast, γ is nearly constant.

Having examined the broadening of the exciton linewidth under the carrier excitation in the barrier, we consider the trapped carrier dynamics. As before, we assume electrons as majority carriers and consider trapping or detrapping of electrons. At low temperature, thermally activated electron emission is negligible. Instead, we take into account the electron emission by photoexcitations. Because of the barrier excitation, the capture of photoexcited holes also occurs. In the steady state, the electron occupation in the trap is thus determined by the rates of electron capture and hole capture under the simultaneous resonant and above-barrier excitations. We use the similar formula as before. Rate equation is now written as $df/dt = (c_e + \pi_o)(1-f) - (c_h + \nu_o)f$. The electron occupation is thus $(c_e + \pi_o)/(c_e + c_h + \nu_o + \pi_o)$, where ν_o and π_o rep-

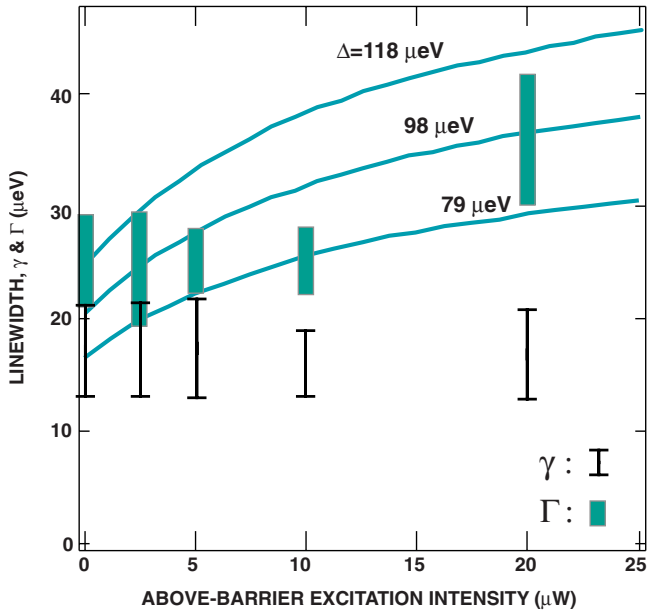

FIG. 11. (Color online) Linewidth contributions γ and Γ obtained for the autocorrelation functions of the QD-2 exciton (Fig. 7) for increasing above-barrier excitation power. Three solid lines show G calculated according to the model described in the text; the upper trace with $n=10^{14}$ cm^{-3}, $\sigma_{eo}=1.3\times10^{-17}$ cm^2, $\sigma_{ho}=2.6\times10^{-17}$ cm^2, $\sigma_e=6\times10^{-15}$ cm^2, and $\sigma_h=1\times10^{-14}$ cm^2. The Stark shift $\Delta=118$, 98, and 79 μeV for the upper, middle, and lower traces, respectively.

resent the photoinduced electron emission and the photoinduced hole emission. The former is induced by the resonant excitation and the latter by the above-barrier excitation, which may be written as $\nu_o=\phi_{\rm res}\sigma_{eo}$ and $\pi_o=\phi_{a.b}\sigma_{ho}$, respectively.[49] The subscripts in the photon fluxes, $\phi_{\rm res}$ and $\phi_{a.b}$, indicate resonant and above-barrier excitation. In Fig. 7, $\phi_{a.b}$ is increased when $\phi_{\rm res}$ is kept constant. At 4 K, the electron capture rate is small; the photoinduced emissions of electrons and holes proceed faster for increasing excitation. For higher excitation, the occupation approaches $\pi_o/(\nu_o+\pi_o)$. The capture cross section may show small thermal activation, but such temperature dependence is negligible at low temperature. We only consider $T^{1/2}$ dependence. The hole capture cross sections are often larger than those of electron capture.[46] The width Γ is now written as $\Delta[(c_e+\pi_o)/(c_e+c_h+\nu_o+\pi_o)]^{1/2}[(c_h+\nu_o)/(c_e+c_h+\nu_o+\pi_o)]^{1/2}$, where Δ is the Stokes shift. In Fig. 11, three calculated Γs are shown as solid lines. In the lower trace, we adopted the background electron density in the barrier of 10^{14} cm^{-3}, $\sigma_{eo}=1.3\times10^{-17}$ cm^2, $\sigma_{ho}=2.6\times10^{-17}$ cm^2, $\sigma_e=6\times10^{-15}$ cm^2, $\sigma_h=1\times10^{-14}$ cm^2, and $\Delta=79$ μeV. For the middle and upper traces Δ was increased, respectively, to 98 and 118 μeV. Overall, the above model for Γ reproduces the experimental results fairly well. The moderate increase in Γ shown above may be due to well-suppressed multiparticle excitation such as biexciton excitation. As will be discussed in Sec. IV, the biexciton excitation leads to the exciton population decay. It is also noteworthy that in QDs whose exciton emissions are observed under barrier excitation, the line broadening becomes significant as the incident density exceeds 90 W/cm^2. Such QDs allow the capture of electrons, holes, and pairs in the barrier. Thus, multiple-carrier capture may easily lead to the exciton population decay. In distinct contrast, above-barrier excitation as high as 20 μW (power density of 640 W/cm^2) is required to observe significant broadening in the present experiment. This density is much larger than the above value by a factor of about seven. We believe that this is due to the suppression of the capture of carriers in the barrier.

Finally in this section, let us recall the correlation decay functions that are featured with the initial fast and the subsequent slower Gaussian decays. We may interpret the features in terms of enhanced exciton-phonon interaction. We can roughly estimate the wave vector of the most efficiently coupled phonons. We take into account only the deformation potential coupling and its longitudinal acoustic (LA) mode. The contribution of transverse acoustic (TA) modes via piezoelectric coupling in QD exciton dephasing is known to be small.[11] For our material system, indium composition is low due to the complex self-assembling process, leading to QD exciton emission energies as high as 1.65–1.68 eV. Thus, we may use the GaAs parameters. The wave vector of the most efficiently coupled phonons is determined by $\max[1/a_B, 1/L]$, where a_B is Bohr radius and L is the effective extent. For QD-2, the energy from the lowest to the first excited states is estimated to be 19 meV. We assume that the (lateral) confinement is approximated by harmonic potential. When confinement energies of electron and hole are, respectively, $\hbar\omega_e=7$ meV and $\hbar\omega_h=3.8$ meV (corresponding localization lengths are 11.7 and 10.0 nm), the lowest to the first excited states is calculated to be $\hbar\omega_e+\hbar\omega_h-E_{ss}+E_{pp}=19.4$ meV, where we introduce direct Coulomb energies, E_{ss}, between the electron and the hole in the s shells, and E_{pp} between those in the p shells. If we disregard the Coulomb energies, confinement with $\hbar\omega_e=12.3$ meV and $\hbar\omega_h=6.6$ meV gives the s-p splitting of 19 meV. In this case, the localization length of the pair is estimated to be 11 nm. Thus, $1/L$ is about 10^6 cm^{-1}, while $1/a_B\sim1.25\times10^6$ cm^{-1}. By adopting the latter value, the cutoff energy is estimated to be 0.4 (0.275) meV for LA (TA) mode, where $\hbar\omega=0.32(0.22)|q|$ meV with $|q|$ scaled in units of 10^6 cm^{-1} was used. The lateral size of a QD is the localization width of the wave function, which is often smaller by a factor of 3 or 4 than the QD diameter. If we regard this, and taking the localization length of 3.5–5 nm, then we have 0.64–0.9 meV for LA mode. At 4 K, k_BT is 0.35 meV. Therefore, both phonon modes are partly occupied. From these expectations, we may consider the decay functions in Fig. 7 as representative of the ZPL and the phonon sideband; the former corresponds to the slowly decaying contribution and the latter to the initial faster decay. The lifetime of the fast component is roughly 150–220 μeV, which overlaps with the cutoff energies estimated above. We may also estimate the weight of the ZPL from the kink in the decay curves that separates the fast and slow contributions. It is about 0.7. This relative weight of the ZPL seems low for a localization length $\sim$10 nm. As references, we find 0.5 at 6 K,[19] 0.4 at 35 K,[32] $\sim$0.75 at 4 K,[28] and 0.9 at 5 K.[50] Specifically, Vagov *et al.*[28] gave a ZPL weight at 4 K of 0.75 for an electron localization length of 11.8 nm. In their estimate, the ground-state-to-

excited-state energy separation seems about 40 meV or more, which is larger than ours (19 meV for 11–12 nm). This may be attributed to the effective mass difference. Thus, to our impression, our value of the weight of ZPL of 0.7 seems rational. We point out that in the present experiment we use continuous-wave excitation, while FWM relies on the pulsed excitation. This difference in excitation may result in difference in phonon environment. We look forward to have discussions with theoreticians. It is now tempting to try a fitting with regard to the ZPL and the sideband. Although we do not have the exact representations of the correlation functions and resulting line shape function of the sideband, we attempt to express the two contributions with an exponential function and an empirical line shape function. We have considered two model line shape functions. In the first model (model A), we use the sideband line shape function that peaks at the most efficiently contributing phonon frequency and decays away for higher energy. The function is shown in the negative detuning region in the inset of Fig. 9. Since it is expected that both the ZPL and the sidebands are subject to the fluctuating environmental perturbation, we multiply a Gaussian decay function to both fast and slow components. The resulting decay is represented by the ZPL weight and the widths, γ_{ZPL} and γ_{SB}, of the ZPL and the sideband, respectively. A result of the fitting is given in Fig. 9; the parameters are $\eta=0.7$, $\gamma_{\mathrm{ZPL}}=9.2$ μeV, $\gamma_R=164$ μeV, $\gamma_F=109$ μeV, and $\Gamma=26.2$ μeV. The parameters γ_R and γ_F, respectively, determine the rise and fall-off of the sideband away from the ZPL energy, and γ_{ZPL} and Γ are the bare width of the ZPL and the broadening parameter as before, respectively. In the second model (model B), we evaluated the line shape $s(\hbar\omega)=\Sigma_p\delta(\hbar\omega-\hbar\omega_p)\varphi^2/(\hbar\omega_p)^3$, where ω is the acoustic-phonon frequency and φ^2 is the angular averaged matrix element of the exciton-phonon interaction. By using the phonon dispersion relation and φ^2 from Ref. 11, we have $s(\hbar\omega)$. It turns out that $s(\hbar\omega)$ is well approximated by an exponential function that decays with increasing energy. We denote the decay parameter as α. By applying Fourier transformation, we have the temporal decay function corresponding to the sideband (fast component). It is summed up with the slowly decaying ZPL exponential function. Again, we multiply a Gaussian to both the fast and slow components. A fitting trial gives $\eta=0.7$, $\gamma_{\mathrm{ZPL}}=9.2$ μeV, $1/\alpha=298$ μeV, and $\Gamma=26.2$ μeV. The resulting spectrum function is shown in the positive detuning region in the inset of Fig. 9, with the magnified sideband contribution. Note that both models give similar spectra with similar sideband tailing. The important point here is that the bare width of the ZPL and the broadening width parameter Γ obtained by the three different models are all close each other, implying that the effect of the fluctuating charges is essential.

D. Resonant excitation power dependences

1. Dephasing due to exciton/biexciton transitions

Finally, we check how the exciton emission spectra behave against the increase in the resonant excitation power. Because the QD-1 exciton shows no appreciable additional broadening under the above-barrier excitation, we may expect that its nearby environment is fairly clean and that the dot is nearly free from fluctuating charges. Thus, QD-1 is a suitable dot for studying the intrinsic dephasing upon increasing photoexcitation resonant to the excited states. Figure 12 depicts three decay functions for the excitation power of 20, 200, and 400 μW at 4 K. The decay at 20 μW (half width of 36 μeV) is very close to that in Fig. 8(a) as expected, and its decay constant is ~18 ps. Surprisingly, for the higher excitations, the decay still follows an exponential function. The time constants are 12.5 and 10 ps, respectively, for 200 and 400 μW. The corresponding half widths are 52.5 and 66 μeV, respectively. The measured half widths are plotted in Fig. 13. The exponential decay strongly suggests that QD-1 is indeed free from the nearby charges. Another claim may be that if they exist, the charge states are not fluctuating. The relevance of this, however, is ruled out: The resonant excitation may induce the photoassisted carrier emission of the charges, if they exist, which will alter the charge state resulting in fluctuation. The decrease in the decay lifetime is then attributed to the increasing dephasing rate. A probable cause is the population decay of the exciton, which is induced by the optical excitation. Such population decay is accompanied by energy change. In the experiment in Figs. 7, 9, and 11, the excess energy of the excitation is

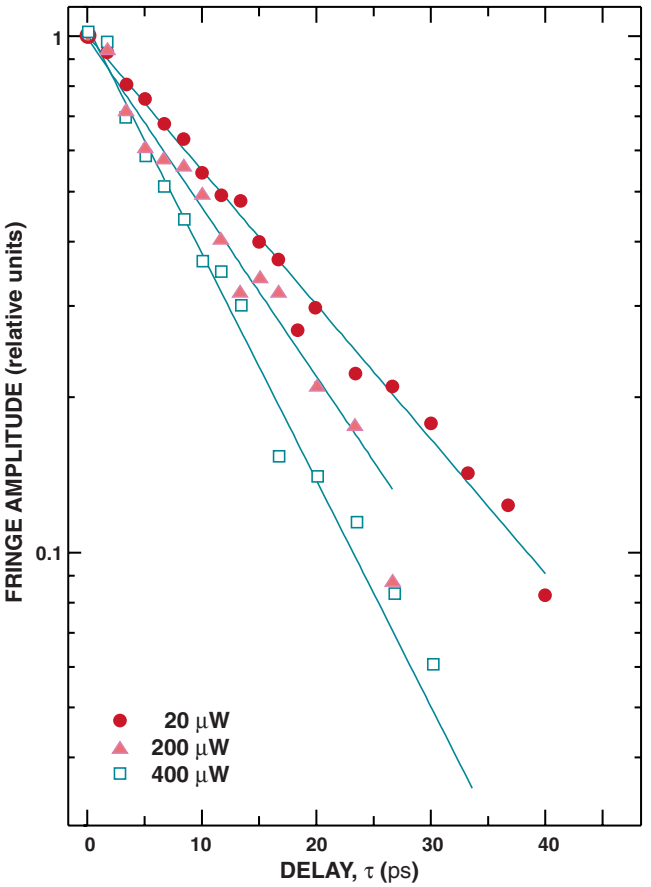

FIG. 12. (Color online) Luminescence autocorrelations of the QD-1 exciton under resonant excitation at 1.768 eV for excitation powers of 20, 200, and 400 μW. The autocorrelation function decays are exponential with a decreasing time constant for increasing power.

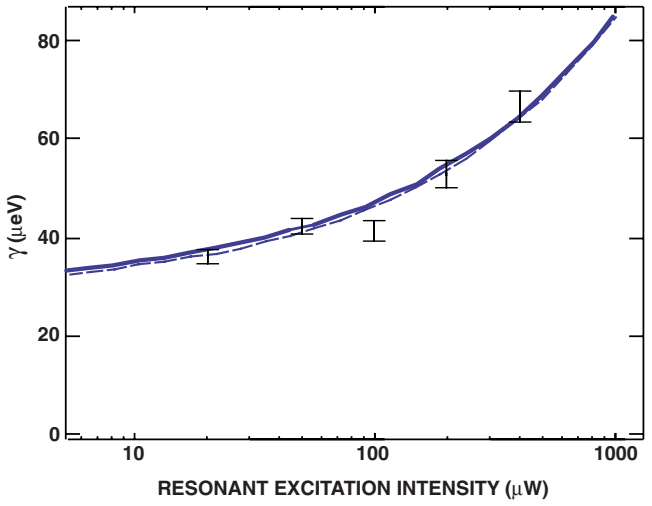

FIG. 13. (Color online) Inverse of decay lifetime of QD-1 exciton luminescence autocorrelation amplitude as a function of the resonant excitation power. Solid and dotted lines are calculated considering the pure dephasing (γ), the spectral diffusion (Γ), and the population decay due to the exciton-biexciton optical transition: Solid line with $\gamma=17$ μeV and $\Gamma=12$ μeV, and dotted line with $\gamma=28.5$ μeV and $\Gamma=0$ μeV. The exciton-biexciton dipole moment of 30 Debye is assumed.

about 95 meV. Then, this continuous-wave excitation not only populates the exciton in an excited state, which subsequently relaxes to the lowest luminescent state, but can also induce the transition from the luminescent state to another state. We now consider biexciton excited states as the final state of the above latter transition from the lowest exciton state. We have already suggested such relevance in the context of the interplay of the optical excitation in the exciton or biexciton system.[34] We now estimate the transition rate from the lowest-energy exciton state to an excited biexcitonic state. Assuming that the transition dipole moment is 30 Debye, then the Rabi (angular) frequency is about 7.6×10^{10} sec^{-1} (half width of 50 μeV) for an excitation density of 25 kW/cm^2. In the experiment, we have 12.7 kW/cm^2 for the excitation of 400 μW (spot size of 1 μm in diameter). Thus for this density, we estimate the Rabi frequency 5.4×10^{10} sec^{-1} (half width of 35.6 μeV and lifetime of 18.4 ps). A rough estimate of the phase decoherence contribution, that is, the decoherence contribution without population decay, can be given by the decay lifetime at the lowest (adopted) power density in Fig. 12: This is the inverse of 18 ps, and thus 5.6×10^{10} sec^{-1} or 36 μeV. Thus, the total rate of the dephasing is about 11×10^{10} sec^{-1} (71.6 μeV), and the corresponding lifetime is 9.2 ps. This is very close to the decay time at the excitation of 400 μW. Therefore, the exciton-biexciton transition as a cause of the exciton dephasing is reasonably acceptable. Shown in Fig. 13 is a result we calculated assuming the pure dephasing width of 28.5 μeV (dotted line, 23 ps of lifetime). We may also take into account of the Gaussian broadening. From the experience in Figs. 5 and 6, we suggest a hidden contribution Γ of the fluctuating charge perturbation, which is estimated to be less than about half the pure dephasing contribution. Accordingly, we estimate $\Gamma<12$ μeV from the smallest width (at the smallest excitation). Correspondingly, the remaining pure dephasing contribution is $\gamma>17$ μeV. As before, we take the dipole moment of 30 Debye for the exciton-biexciton (excited) transition, and we assume $\gamma=17$ μeV and $\Gamma=12$ μeV. The sum of these three rates gives a solid line in Fig. 13; the difference between the two calculations is subtle. The overall agreement is therefore confirmed. We attribute the exciton-biexciton transition to the extra exciton line broadening at high-density resonant excitation.

E. Contributions to the exciton linewidth

The contribution of the pure dephasing was theoretically estimated for larger QDs of few ten nanometers at about 4 K, and is about 15 μeV in half width, which corresponds to about 44 ps.[11] In our QDs, the as-measured half width was 31–36 μeV, while the measured radiative decay lifetime is about 220 ps, giving only 1.5-μeV contribution to the half width. Therefore, [(31–36) μeV−1.5 μeV−15 μeV] the difference between the as-measured width and the sum of the radiative population decay width and the pure dephasing is about 11.5–16.5 μeV. We have shown that the fast spectral diffusion due to the random interaction between the excitons and the fluctuating neighboring trapped charges amounts to 10–25 μeV, depending on the (estimated) distance between the exciton and charge and on temperature. Namely, for QD-2, the as-measured half width at 4 K is 28–30 μeV and the radiative width is 1.5 μeV. The experiment and the fitting discriminate the dephasing of 10 μeV and the extra broadening of 20–25 μeV due to the spectral diffusion. Their sum indeed agrees with the as-measured half width, although simple addition is not appropriate. The 10 μeV of the dephasing may be further decomposed to the radiative width of 1.5 ps and the pure dephasing width of 8.5 μeV. Therefore, the accounting of the stochastic interaction between exciton and nearby charges and the resulting spectral diffusion and broadening well explain the experimental results on the exciton line shape and first-order correlation function.

F. Remarks

In conclusion, we have presented a detailed analysis of the line broadening of single-dot exciton emissions in terms of fluctuating interaction between the QD exciton and environmental trapped charges. We examined two types of QD excitons: one accompanied by trapped charge, whereby the exciton line redshifts under the trapped charge population, and the other nearly free from trapped charges. In order to highlight the effect of the fluctuating charges, and to avoid population decay of exciton—which results from multiple-carrier capture into the QDs, thereby leading to line broadening—we selected QDs that reject the capture of carriers in the barrier material. Interferometric correlation measurements of the single-dot emissions uncover the importance of the trapped charges near the QDs. We have demonstrated that the absence or presence of nearby charges largely modifies the interference correlation function: The fluctuation of the Coulomb field caused by the trapping or detrapping of charges in point defects changes the autocor-

relation function into Gaussian decay. In contrast, in the QD nearly free from the trapped nearby charges, the autocorrelation decay obeys a simple exponential function, which is consistent with the absence of the fluctuating charge perturbation. Therefore, the accounting of the stochastic interaction between exciton and nearby charges and the resulting spectral diffusion and broadening well explain the experimental results on the exciton line shape and first-order correlation function. By identifying the fluctuating environmental charges as significant cause of single-dot exciton luminescence line broadening, we can now explain why one observes a substantial extra broadening in single-exciton zero-phonon line spectrum, in addition to the dephasing contribution that arose from pure dephasing and radiative population decay.

Interestingly, for the QD exciton that exhibits substantial redshift upon the carrier creation in the barrier, such an effect is substantial: As the dephasing rate increases as a result of the temperature rise, and finally overwhelms the random environmental fluctuation effect, the correlation function becomes exponential. In that phenomenon, the estimated random-fluctuation-induced broadening contribution Γ does not show appreciable change against the temperature rise. It is noteworthy that a motional narrowing effect on the QD exciton linewidth has recently been reported. Motional narrowing refers to the phenomenon where the resonance line of a system coupled to a reservoir becomes narrower with increasing reservoir fluctuation. It has been claimed that motional narrowing occurs when decreasing incident power or temperature is decreased. In contrast, our results indicate that relative significance of the randomly fluctuation-induced broadening to the dephasing simply determines whether the decay function obeys an exponential or a Gaussian function.

More interestingly, when the excitation energy is changed and the carriers are intensively created in the barrier material, the correlation function seems to change into a decay function featuring an initial fast decay followed by a slow decay as a Gaussian function. The decay constant, however, only slightly increases for higher excitation. We suggest that this moderate increase in the broadening purely represents the effect of the fluctuating environment charges. Due to the potential profiles surrounding the QDs, which were indeed strategically chosen to prevent multiple-carrier capture into the QDs, we only observed spectrum broadening due to the frequent diffusion of the emission energy. In distinct contrast, in the QDs free from the nearby charges, the random-fluctuation-induced broadening is absent or undetected. The autocorrelation function is absolutely exponential. The intense resonant excitation of ~ 100 kW/cm^2 results in a shortening of the coherence lifetime. This is well explained by the population decay of the lowest-lying exciton population induced by the optical transition to the excited biexcitonic states.

The characteristic decay function with the fast and slow parts observed for QD-2 infer the relevance of the ZPL and the sideband. Careful examination rules out artifacts caused by time resolution, suggesting the relevance of the photon emission processes accompanying absorption or emission of phonon. Numerical fitting with the fast- and slow-decaying exponentials (the Gaussian decay function is multiplied to account for the random fluctuation) reproduces very well the observed decay curve. However, such fittings are still awaiting an exact understanding of the line shape of the sidebands, which hopefully may be given theoretically. It is noteworthy that the appearance of the specific decay functions feature by the ZPL and sidebands depends on the dots. It is suggested that the degree of the exciton localization may affect whether or not the phonon sidebands emerge. In the present experiments, however, the lateral extent of the QDs was larger than 20 nm. Existing theories, which predict such satellite phonon-related structures, assume fairly small QDs, such as the QDs of 3, 6, and 12 nm in extent.[51,52] The dephasing rates in our experiments do not substantially differ from each other, and the overall behaviors of the exciton luminescences seem similar. Nevertheless, one shows the sidebands and the others do not. It has been shown that a static electric field may result in a pronounced dephasing via the polar interaction.[51] In high fields, piezoelectric and deformation potential interactions may reach comparable strength. In our QD-2, the nearby trapped charges in fact exert a fluctuating electric field, while the autocorrelation of the exciton emission shows a pronounced weight of the phonon sidebands relative to the ZPL. While the theory predicts that the electric field shortens the dephasing time,[51] the values γ (the dephasing time) and η (the relative weight) obtained by the fitting only vary by 5% for increasing excitation intensity, showing no systematic change. Thus, at present, we cannot give any conclusive reasoning for the appearance of the phonon-related structures. Further study may elucidate the factors that determine the phonon-related spectral shape of the QD emission.

ACKNOWLEDGMENTS

We express sincere thanks to K. Naganuma for his advice on interferometer constructon. We acknowledge S. Hughes, H. Gotoh, and J. Yumoto for helpful discussions and useful comments.

[1] X. Li, Y. Wu, D. Steel, D. Gammon, T. H. Stievater, D. S. Katzer, D. Park, C. Piermarocchi, and L. J. Sham, Science **301**, 809 (2003).

[2] M. V. Gurudev Dutt, J. Cheng, Y. Wu, X. Xu, D. G. Steel, A. S. Bracker, D. Gammon, S. E. Economou, R. B. Liu, and L. J. Sham, Phys. Rev. B **74**, 125306 (2006).

[3] N. H. Bonadeo, J. Erland, D. Gammon, D. Park, D. S. Katzer, and D. G. Steel, Science **282**, 1473 (1998).

[4] T. H. Stievater, Xiaoqin Li, D. G. Steel, D. Gammon, D. S. Katzer, D. Park, C. Piermarocchi, and L. J. Sham, Phys. Rev. Lett. **87**, 133603 (2001).

[5] H. Kamada, H. Gotoh, J. Temmyo, T. Takagahara, and H. Ando,

Phys. Rev. Lett. **87**, 246401 (2001).
[6] H. Htoon, T. Takagahara, D. Kulik, O. Baklenov, A. L. Holmes, Jr., and C. K. Shih, Phys. Rev. Lett. **88**, 087401 (2002).
[7] P. Borri, W. Langbein, S. Schneider, U. Woggon, R. L. Sellin, D. Ouyang, and D. Bimberg, Phys. Rev. Lett. **87**, 157401 (2001).
[8] W. Langbein, P. Borri, U. Woggon, V. Stavarache, D. Reuter, and A. D. Wieck, Phys. Rev. B **70**, 033301 (2004).
[9] D. Birkedal, K. Leosson, and J. M. Hvam, Phys. Rev. Lett. **87**, 227401 (2001).
[10] See, for example, T. Takagahara, in *Quantum Coherence, Correlation and Decoherence in Semiconductor Nanostructure*, edited by T. Takagahara (Academic, New York, 2003).
[11] T. Takagahara, Phys. Rev. B **60**, 2638 (1999).
[12] D. Gammon, E. S. Snow, B. V. Shanabrook, D. S. Katzer, and D. Park, Science **273**, 87 (1996).
[13] D. Gammon, E. S. Snow, B. V. Shanabrook, D. S. Katzer, and D. Park, Phys. Rev. Lett. **76**, 3005 (1996).
[14] N. H. Bonadeo, Gang Chen, D. Gammon, D. S. Katzer, D. Park, and D. G. Steel, Phys. Rev. Lett. **81**, 2759 (1998).
[15] Eiichi Hanamura, Phys. Rev. B **38**, 1228 (1988).
[16] D. Birkedal, K. Leosson, and J. M. Hvam, Superlattices Microstruct. **31**, 97 (2002).
[17] K. Leosson, J. R. Jensen, J. M. Hvam, and W. Langbein, Phys. Status Solidi B **221**, 49 (2000).
[18] C. Kammerer, G. Cassabois, C. Voisin, M. Perrin, C. Delalande, Ph. Roussignol, and J. M. Gérard, Appl. Phys. Lett. **81**, 2737 (2002).
[19] V. Zwiller, T. Aichele, and O. Benson, Phys. Rev. B **69**, 165307 (2004).
[20] M. Bayer and A. Forchel, Phys. Rev. B **65**, 041308(R) (2002).
[21] H. Gotoh, H. Ando, H. Kamada, A. Chavez-Pirson, and J. Temmyo, Appl. Phys. Lett. **72**, 1341 (1998).
[22] C. Santori, G. S. Solomon, M. Pelton, and Y. Yamamoto, Phys. Rev. B **65**, 073310 (2002).
[23] Ph. Roussignol, W. Heller, A. Filoramo, and U. Bockelmann, Physica E (Amsterdam) **2**, 588 (1998).
[24] V. Zwiller, M.-E. Pistol, D. Hessman, R. Cederström, W. Seifert, and L. Samuelson, Phys. Rev. B **59**, 5021 (1999).
[25] D. V. Regelman, E. Dekel, D. Gershoni, W. V. Schoenfeld, and P. M. Petroff, Phys. Status Solidi B **224**, 343 (2001).
[26] E. A. Muljarov and R. Zimmermann, Phys. Rev. Lett. **93**, 237401 (2004).
[27] P. Machnikowski, Phys. Status Solidi B **243**, 2247 (2006).
[28] A. Vagov, V. M. Axt and T. Kuhn, W. Langbein, P. Borri, and U. Woggon, Phys. Rev. B **70**, 201305(R) (2004).
[29] R. G. Neuhauser, K. T. Shimizu, W. K. Woo, S. A. Empedocles, and M. G. Bawendi, Phys. Rev. Lett. **85**, 3301 (2000).
[30] H. D. Robinson and B. B. Goldberg, Phys. Rev. B **61**, R5086 (2000).
[31] I. Chung and M. G. Bawendi, Phys. Rev. B **70**, 165304 (2004).
[32] A. Berthelot, I. Favero, G. Cassabois, C. Voisin, C. Delalande, Ph. Roussibnol, R. Ferreira and J. M. Gérard, Nat. Phys. **2**, 759 (2006).
[33] A model is given in Ref. 26 of QD ionization as the mechanism for the blinking event, followed by a redistribution of local electric fields that results in spectral shifting.
[34] Mitsuru Sugisaki, Hong-Wen Ren, Kenichi Nishi, and Yasuaki Masumoto, Phys. Rev. Lett. **86**, 4883 (2001).
[35] S. Adachi, N. Yatsu, R. Kaji, S. Muto, and H. Sasakura, Appl. Phys. Lett. **91**, 161910 (2007).
[36] R. Nötzel, J. Temmyo, and T. Tamamura, Nature (London) **369**, 131 (1994).
[37] H. Kamada, H. Ando, J. Temmyo, and T. Tamamura, Phys. Rev. B **58**, 16243 (1998).
[38] H. Gotoh and H. Ando, J. Appl. Phys. **82**, 1667 (1997).
[39] H. Gotoh, H. Kamada, H. Ando, and J. Temmyo, Appl. Phys. Lett. **76**, 867 (2000).
[40] H. Gotoh, H. Kamada, T. Saitoh, H. Ando, and J. Temmyo, J. Appl. Phys. **94**, 342 (2003).
[41] S. I. Pokutnyi, L. Jacak, J. Misiewicz, W. Salejda, and G. G. Zegrya, J. Appl. Phys. **96**, 1115 (2004).
[42] V. Stavarache, D. Reuter, A. D. Wieck, M. Schwab, D. R. Yakovlev, R. Oulton, and M. Bayer, Appl. Phys. Lett. **89**, 123105 (2006).
[43] M. M. Vogel, S. M. Ulrich, R. Hafenbrak, P. Michler, L. Wang, A. Rastelli, and O. G. Schmidt, Appl. Phys. Lett. **91**, 051904 (2007).
[44] A. V. Uskov, A.-P. Jauho, B. Tromborg, J. Mork, and R. Lang, Phys. Rev. Lett. **85**, 1516 (2000).
[45] P. W. Anderson and P. R. Weiss, Rev. Mod. Phys. **25**, 269 (1953).
[46] C. H. Henry and D. V. Lang, Phys. Rev. B **15**, 989 (1977).
[47] H. Kamada, J. Temmyo, M. Notomi, T. Furuta, and T. Tamamura, Jpn. J. Appl. Phys., Part 1 **36**, 4194 (1997).
[48] R. Kubo, in *Fluctuation, Relaxation and Resonance in Magnetic Systems*, edited by D. ter Haar (Oliver and Boyd, Edinburgh, 1962).
[49] H. Kukimoto, C. H. Henry, and F. R. Merritt, Phys. Rev. B **7**, 2486 (1973).
[50] P. Borri, W. Langbein, U. Woggon, V. Stavarache, D. Reuter, and A. D. Wieck, Phys. Rev. B **71**, 115328 (2005).
[51] B. Krummheuer, V. M. Axt, and T. Kuhn, Phys. Rev. B **65**, 195313 (2002).
[52] L. Jacak, J. Krasnyj, W. Jacak, R. Gonczarek, and P. Machnikowski, Phys. Rev. B **72**, 245309 (2005).